Revision 3

The $MnCO_3$- II high pressure polymorph of rhodocrosite

Marco Merlini[1,*], Michael Hanfland[2], Mauro Gemmi[3]

[1]Dipartimento di Scienze della Terra, Università degli Studi di Milano, via Botticelli 23, 20133 Milano, Italy

[2]European Synchrotron Radiation Facility, BP 220, 38043 Grenoble, Cedex 9, France

[3]Center for Nanotechnology Innovation@NEST, Istituto Italiano di Tecnologia, I-56127 Pisa, Italy

*corresponding author: marco.merlini@unimi.it

Abstract

We investigated the behavior of $MnCO_3$ in the pressure range 0-50 GPa and ambient temperature by synchrotron X-ray single crystal diffraction technique. $MnCO_3$ maintains the calcite-type structure (*R*-3*c* symmetry) up to 44 GPa. Above this pressure we observed a phase transition. The high pressure phase, $MnCO_3$-II, is triclinic, with cell parameters a=2.928(2) Å, b=4.816(4) Å, c=5.545(4) Å, α=101.71(6)°, β=94.99(6)°, γ=89.90(6)°, Vol=76.28(10) $Å^3$ at 46.8 GPa. The structure is solved with the charge flipping algorithm. $MnCO_3$-II is isostructural with $CaCO_3$-VI. The density increase on phase transition is 4.4%. The occurrence of $CaCO_3$-VI structure in $MnCO_3$ composition indicates that $CaCO_3$-VI structure is also adopted by carbonates with cations smaller than calcium.

Introduction

The structural behavior of carbonates at high pressure, can provide insights into the crystal chemistry of carbonates at the Earth's mantle conditions. The evidence of structural transitions at non ambient conditions (i.e. Oganov et al. 2013) indicates that the polymorphism of carbonates is perhaps more complex than it is currently considered. Therefore, structural investigations on the various polymorphs adopted by carbonates are important studies aimed at a better understanding of the carbonate crystal chemistry in the inner Earth.

The mineral rhodocrosite, $MnCO_3$, at ambient conditions, crystallizes with the calcite-type structure, *R*-3*c* (Wyckoff 1920). Ono (2007) reported a phase transition at 50 GPa, after heating at 1500-2000 K. $MnCO_3$ was observed to be stable in its rhombohedral calcite-type structure up to those pressures, as confirmed by the work performed by Santillan and Williams (2004), who did not observed any transition up to 45-50 GPa. Farfan et al. (2013), reported a possible electronic transition in rhodochrosite, related to Mn behavior, in the pressure interval 25-40 GPa. They propose a possible change in symmetry. These authors also observed a change in the rhodocrosite powder pattern above 50 GPa.

In order to clarify some of these issues related to $MnCO_3$ behavior at non ambient conditions, we performed a single crystal study of rhodochrosite at high pressure in the interval 0-45 GPa. In the following sections we report the results based on

structural refinements for each pressure step, and the structure solution achieved for $MnCO_3$-II, the high pressure polymorph observed above 43 GPa at ambient temperature.

Materials and methods

Natural samples of rhodocrosite from Sardegna (Italy) were used for the high pressure experiments. Microprobe analysis was performed with a Jeol Superpobe instrument (Earth Science Department, University of Milano), which indicated an almost pure $MnCO_3$ end-member, with a minor Ca content, resulting in a $Mn_{0.96}Ca_{0.04}CO_3$ formula. A prescreening single crystal diffraction performed with an Oxford diffraction instrument (Earth Science Department, University of Milano) confirmed the rhombohedral *R*-3*c* calcite-type structure for the sample.

The high pressure experiments were performed with a membrane-type Diamond anvil cell at the ID09A beamline of ESRF, The European Synchrotron (Grenoble, France). The standard beamline setup was used as reported in Merlini and Hanfland (2013), with a monochromatic beam (λ=0.41432 Å) and a spot size of approximately 30x30 μm^2 on the sample.

Two experimental runs were performed in the high and low pressure range respectively. The high pressure run was collected using a 300 μm culet diameter cell, Re gasket and Ne as pressure transmitting medium. After one measurement at ambient condition the gas was loaded in the cell and the pressure rapidly raised to 18 GPa. Then, single crystal data diffraction data were collected on increasing pressure every 1.5 GPa. Pressure was monitored with Ne diffraction (Fei et al. 2007) and ruby

fluorescence scale (Mao et al. 1986). The difference between the two pressure sensors is negligible.

A second run in the low pressure range (0-25 GPa) was performed, using a 600 μm culet diameter cell, stainless steel gasket and He as pressure transmitting medium. Single crystal diffraction data sets were collected by omega axis rotations (Busing and Levy 1967), integrating each frames on 1° step size in the angular interval -30°/+30°. As soon as a phase transition was detected above 43 GPa, reciprocal space sampling was increased by collecting data at different chi axis positions, to access all the available reciprocal space allowed by the diamond anvil cell opening cone.

Raw single crystal data were handled by the Crysalis software (Oxford Diffraction, 2008), extracting lattice parameters and intensity data. Crystal structure analysis was performed with the Jana2006 software (Petricek et al. 2014). Structure solution was achieved with the Superflip (Palatinus and Chapuis 2007) program and successive Fourier difference analysis.

Results

High pressure behavior of *R*-3*c* $MnCO_3$

The crystal structure of $MnCO_3$ at ambient conditions is in agreement with literature data (Graf 1961; Maslen et al. 1995). It is calcite-type, *R*-3*c*, where layers of Mn cations alternate with parallel $(CO3)^{2-}$ groups. Mn features an octahedral coordination. The geometry of the MnO_6 octahedra results in six equal Mn-O distances, and two sets of variable O-O edge distances and O-Mn-O angles. The difference between the O-O edge distances is related to the deviation from a regular octahedron.

The diffraction peaks in the pressure range 0-41 GPa are indexed with a rhombohedrally centred hexagonal unit cell (table 1). No deviation from unit cell angles α=90° and γ=120° are detected within experimental accuracy, suggesting that, metrically, the rhodocrosite sample retains the rhombohedral lattice up to 41 GPa at ambient temperature. The volume data are fitted to a 3rd order Birch-Murnagham equation of state, resulting in bulk modulus K_0=110(3) GPa, K'=3.8(2) and V_0=310.4(5) Å^3 or K_0=106.9(11) and V_0=310.7(4) Å^3 if a 2nd order BM-EoS is used (Figure 1). The analysis of the f-F plot (Angel 2000) indicates that a 4th order BM EoS is not necessary for fitting the experimental data (Deposit Item) despite the large

pressure range investigated. The compressibility is anisotropic, with the *c* axis markedly more compressible than the *a* axis (Figure 2).

The crystal structure of rhodocrosite can be described with the calcite-type *R*-3*c* structure during the entire 0-41 GPa pressure range, and no significant change in R agreement factor is observed at high pressure (Deposit Item).

As a result of compression, the interatomic Mn-O and C-O distances shrink, with the C-O bond behaving more rigidly (Figure 3). The MnO_6 coordination polyhedron is not regular, and its distortion can be described either by the bond angles, or, more immediately, by the two O-O edge distances (Lavina et al. 2010). In Figure 4 these distances are reported as function of pressure, and they indicate that around 15 GPa the octahedron is quite regular, with a shape more elongated along the *c* axis in the lower pressure range and more compressed in the higher pressure range.

The crystal structure of $MnCO_3$-II above 43 GPa

Above 43 GPa, a phase transition is observed. The rotation diffraction image (Figure 5) clearly indicates the presence of additional features if compared to lower pressure ones. In addition, we notice the presence of significant diffuse scattering. The diffraction peaks are indexed on the basis of a triclinic lattice (Table 1), which is remarkably similar to the unit cell of $CaCO_3$-VI (Merlini et al. 2012a). The integrated

hkl-intensities are reliable for a structure solution with the charge flipping algorithm completed by a Fourier difference analysis for the location of carbon atoms. The structure refinement demonstrates that $MnCO_3$-II is isostructural with $CaCO_3$-VI. The structure has two formula units in the unit cell, related by an inversion centre, for a total of five atoms in the asymmetric unit. All the atoms are in general positions. $MnCO_3$-II is 5% denser than rhodocrosite, and, from a structural point of view, the density increase is explained by an increased coordination number of Mn atoms. The resulting [7]-fold coordination polyhedron is approximately a distorted trigonal prism, with a pyramidal termination on a long face (Figure 5). The Mn-O distances are in the range 2.0-2.26 Å. The CO_3 groups, whose geometry is unconstrained by the crystal symmetry, still retain a planar configuration, with C-O distances in the range 1.15-1.3 Å (table 2). The $MnCO_3$ to $MnCO_3$-II phase transition is reversible, and pressure release reconverts the sample in rhodocrosite structure, with a small hysteresis observed.

Discussion, implications and concluding remarks

We report here new experimental data that help a further understanding of the high pressure behavior of $MnCO_3$. The current results, based on single crystal structural analysis, with sample maintained in a quasi-hydrostatic medium (Ne) clearly indicate that the calcite-type structure is maintained up to 43 GPa. Above this pressure, it transforms to a higher pressure polymorph. This is fairly in agreement with all the previous reports, in particular with Ono (2007) and Farfan et al. (2013), who describe a phase transition near 50 GPa. The stability of *R*-3*c* structure in a wide pressure range agrees also with Santillan and Williams 2004. The pressure interval (0-40 GPa) of the current experiments, overlaps with the recent observations of the behavior of $MnCO_3$ by Farfan et al. (2013). We notice that the experimental conditions are quite differents, in particular single crystal in Ne pressure medium (current data) vs. powder in NaCl pressure transmitting medium (Farfan et al. 2013). It is known that NaCl undergoes a first order phase transition around 30 GPa, from NaCl-type to CsCl-type structure, with important volume change (Bassett et al. 1968; Bridgman 1970; Jeanloz and Li 1987). It is not surprisingly that those experimental conditions have introduced strain with consequent difficulties in fitting the powder pattern with undistorted rhombohedral lattice. However, the suggestion that an electronic Mn state can change in the pressure interval 15-50 GPa is mostly derived from spectroscopic (Raman) investigation. We notice, based on structure refinements, a structural change in local Mn environment. The MnO_6 octahedra are elongated parallel to the c axis in

the low pressure region. They become regular at 15 GPa, and, above, they turn elongated parallel to the a-b plane (Figure 4). This behavior is similar to siderite (Lavina et al. 2010). This fine structural details may actually couple with a change in the Mn electronic configuration, as suggested by Farfan et al. 2013. The current single crystal data, however, indicate that, if present, a possible Mn electronic transition do not produce discontinuities in symmetry and structural parameters, at least within the X-ray sensitivity achievable with the current experimental accuracy.

Above 43 GPa a first order transition is observed. The first order character is demonstrated both by the volume discontinuity and the hysteresis observed in back-transformation on pressure release.

The discrepancy in the phase transition pressure between this paper and the works of Farfan et al. (2013) and Ono (2007) can be ascribed to the single crystal vs. powder diffraction observations. It has been noticed several times (Merlini et al. 2009; 2012b) that powder samples and single crystal samples behave differently upon first order transition, with powder samples expanding their metastability field. Single crystal, on the contrary, transforms rapidly. This may explain the few GPa difference between our detected transition (44 GPa) and those slightly higher in other studies and the lack of phase transition up to 47 GPa in Santillan and Williams (2004) work. Another possible source of discrepancies could be the variable crystal chemistry of the sample used in the different studies.

$MnCO_3$-II polymorph is different from the high pressure polymorph of Ono (2007), stabilized at 50 GPa after laser heating, whose powder pattern cannot be indexed with the $MnCO_3$-II triclinic phase. This is a clear indication that the phase diagram is rather complex, with a high pressure and low temperature phase, $MnCO_3$-II, and a still unknown high pressure and high temperature polymorph.

The $MnCO_3$-II structure demonstrates that the $CaCO_3$-VI structure (Merlini et al. 2012a; Oganov et al. 2006; 2013) can be adopted also by carbonates hosting smaller cations than calcium, Mn here specifically. We may therefore speculate about a possible miscibility between $CaCO_3$ in its high pressure forms and other components, such as $MnCO_3$ or, more interestingly for the inner Earth, $MgCO_3$ and $FeCO_3$. $CaCO_3$-VI presents a competitive energy (Oganov et al. 2013) compared to aragonite, and, if a mixture between $CaCO_3$ and other components could be established and its free energy would be lower than aragonite , then this simple and dense polymorph may possess an interesting thermodynamic stability field at intermediate pressures. A possibility worthwhile for further investigations.

Acknowledgments

We acknowledge A. Risplendente, N. Rotiroti and G.D. Gatta for assistance in microprobe and single crystal diffraction analysis at Earth Science Department, Università degli Studi di Milano. We acknowledge I. Loa for the use of *Mar4Crysalis* software. DCO (Deep Carbon Observatory) is acknowledged for supporting this research. ESRF is acknowledged for provision of beamtime within the proposal HS-4720.

References

Angel, R.J. (2000) Equation of state. Reviews in Mineralogy and Geochemistry, 41, 35-60.

Bassett, W.A., Takahashi T., Mao H.K., Weaver J.S. (1968) Pressure Induced Phase Transformation in NaCl. Journal of Applied Physics, 39, 319.

Bridgman, P.W. The Physics of High Pressure. Dover, New York, 1970.

Busing, W.R. and Levy, H.A. (1967) Angle calculations for 3- and 4-circle X-ray and neutron diffractometers. Acta Crystallographica, 22, 457-464.

Farfan, G.A., Boulard, E., Wang, S. Mao, W.L. (2013) Bonding and electronic changes in rhodochrosite at high pressure. American Mineralogist, 98, 1817–1823.

Fei Y., Ricolleau, A., Frank, M., Mibe K., Shen, G., Prakapenka, V. (2007) Toward an internally consistent pressure scale. Proceedings of the National Academy of Sciences of the U.S.A., 104, 9182-9186.

Graf, D.L. (1961) Crystallographic tables for the rhombohedral carbonates. American Mineralogist 46, 1283-1316.

Jeanloz, R., Li, X. (1987) Measurement of the B1-B2 transition pressure in NaCl at high temperatures. Physical Review B., 36, 474.

Lavina, B., Dera, P., Downs, R., Yang, W., Sinogeikin, S., Meng, Y., Shen, G., and Schiferl, D. (2010) Structure of siderite $FeCO_3$ to 56 GPa and hysteresis of its spin-pairing transition. Physical Review B, 82, 064110.

Mao, H.K., Xu, J., and Bell, P.M. (1986) Calibration of the ruby pressure gauge to 800 kbar under quasi-hydrostatic conditions. Journal of Geophysical Research, 91, 4673–4676.

Maslen, E.N., Streltsov, V.A., Streltsova, N.R., Ishizawa, N. (1995) Electron density and optical anisotropy in rhombohedral carbonates. III. Synchrotron X-ray studies of $CaCO_3$, $MgCO_3$ and $MnCO_3$. Acta Crystallographica B51, 929-939.

Merlini, M., Gemmi, M., Hanfland, M., Crichton W.A.C (2009) High-pressure behavior of åkermanite and gehlenite and phase stability of the normal structure in melilites. American Mineralogist 94, 704-709.

Merlini, M., Hanfland, M. (2013) Single-crystal diffraction at megabar conditions by synchrotron radiation. High Pressure Research, 33, 511-522.

Merlini, M., Hanfland, M., and Crichton, W.A. (2012a) $CaCO_3$-III and $CaCO_3$-VI, high-pressure polymorphs of calcite: Possible host structures for carbon in the Earth's mantle. Earth and Planetary Science Letters, 333, 265–271.

Merlini, M., Perchiazzi, N., Hanfland, M., Bossak A. (2012b) Phase transition at high pressure in $Cu_2CO_3(OH)_2$ related to the reduction of the Jahn-Teller effect. Acta Crystallographica Section B: Structural Science, 68, 266-274

Oganov, A.R., Glass, C.W., and Ono, S. (2006) High pressure phases of $CaCO_3$: crystal structure prediction and experiment. Earth and Planetary Science Letters, 241, 95-103.

Oganov, A.R., Hemley, R.J., Hazen, R.M., Jones, A.P. (2013) Structure, bonding, and mineralogy of carbon at extreme conditions. Reviews in Mineralogy and Geochemistry, 75, 47-77.

Ono, S. (2007) High-pressure phase transformation in $MnCO_3$: a synchrotron XRD study. Mineralogical Magazine, 71, 105-111.

Oxford Diffraction (2008) CrysAlis RED, Version 1.171.32.29. Oxford Diffraction, Abingdon, England.

Palatinus, L., Chapuis, G. (2007) SUPERFLIP – a computer program for the solution of crystal structures by charge flipping in arbitrary dimensions. Journal of Applied Crystallography, 41, 786–790.

Petricek, V., Dusek, M. & Palatinus, L. (2014) Crystallographic computing system JANA2006: General features. Zeitschrift fur Kristallographie 229(5), 345-352.

Santillán, J., Williams, Q. (2004). A high-pressure infrared and X-ray study of $FeCO_3$ and $MnCO_3$: comparison with $CaMg(CO_3)_2$-dolomite. Physics of the Earth and Planetary Interiors, 143–144, 291–304.

Wyckoff, R. (1920) The crystal structures of some carbonates of the calcite group. American Journal of Science, 50, 317-360.

266

Figure captions

Figure 1 – Unit cell volume per formula unit (V/Z) of $MnCO_3$. The rhodochrosite data are fitted with a Birch-Murnagham EoS.

Figure 2 – Pressure evolution of normalized lattice parameters of rhodocrosite, $MnCO_3$

Figure 3- Mn-O and C-O bond distances as function of pressure.

Figure 4 – Edge distances of MnO_6 octahedra in $MnCO_3$. O-O' is perpendicular to the crystallographic c axis, O-O'' is parallel.

Figure 5- (a) diffraction image during a 60° rotation, showing the sharp diffraction peaks of rhodocrosite at 41 GPa; (b) diffraction rotation image of $MnCO_3$-II 46.8 GPa, showing diffractions and and diffuse scattering; (c) Crystal structure of $MnCO_3$-II

Table 1 – Crystallographic data of $MnCO_3$. *after 1 day. †only lattice parameter determination.

Table 2 – Crystallographic data and selected interatomic distances for MnCO3-II at 46.8 GPa

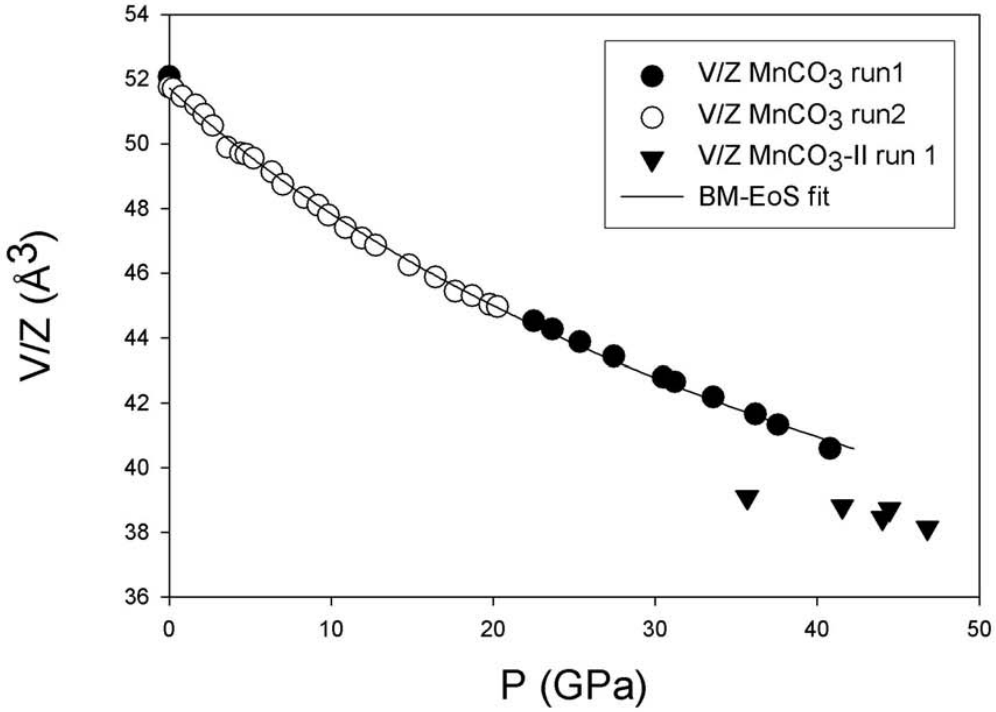
V/Z MnCO3 run1
V/Z MnCO3 run2
V/Z MnCO3-II run 1
BM-EoS fit
V/Z (Å3)
P (GPa)
54
52
50
48
46
44
42
40
38
36
0
10
20
30
40
50

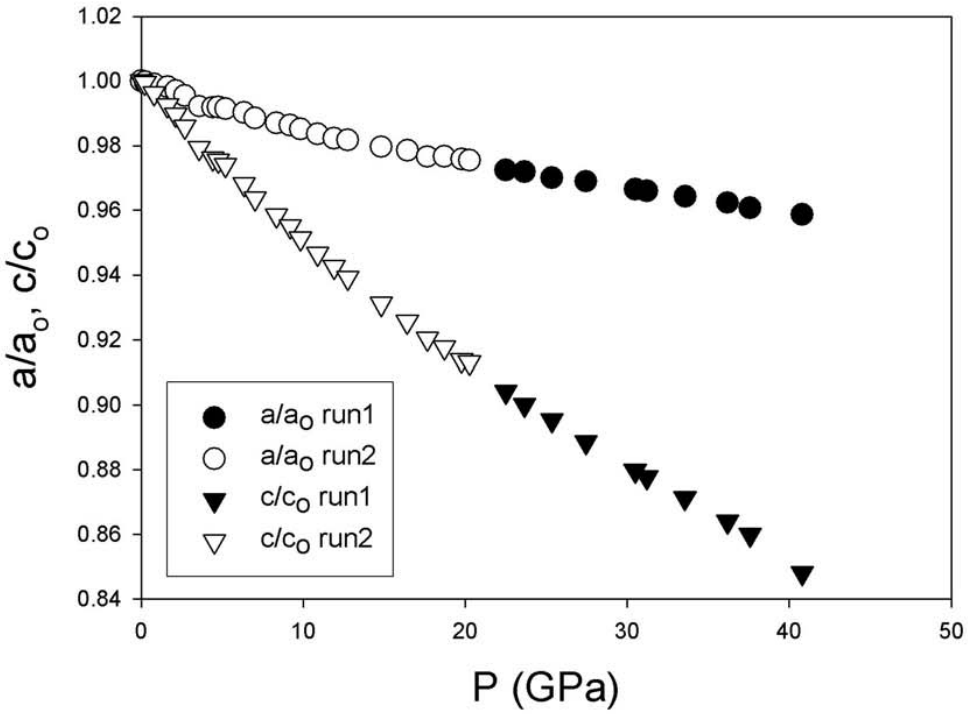
1.02
1.00
0.98
0.96
0.94
0.92
0.90
0.88
0.86
0.84
a/a$_o$, c/c$_o$
0
10
20
30
40
50
P (GPa)
a/a$_o$ run1
a/a$_o$ run2
c/c$_o$ run1
c/c$_o$ run2

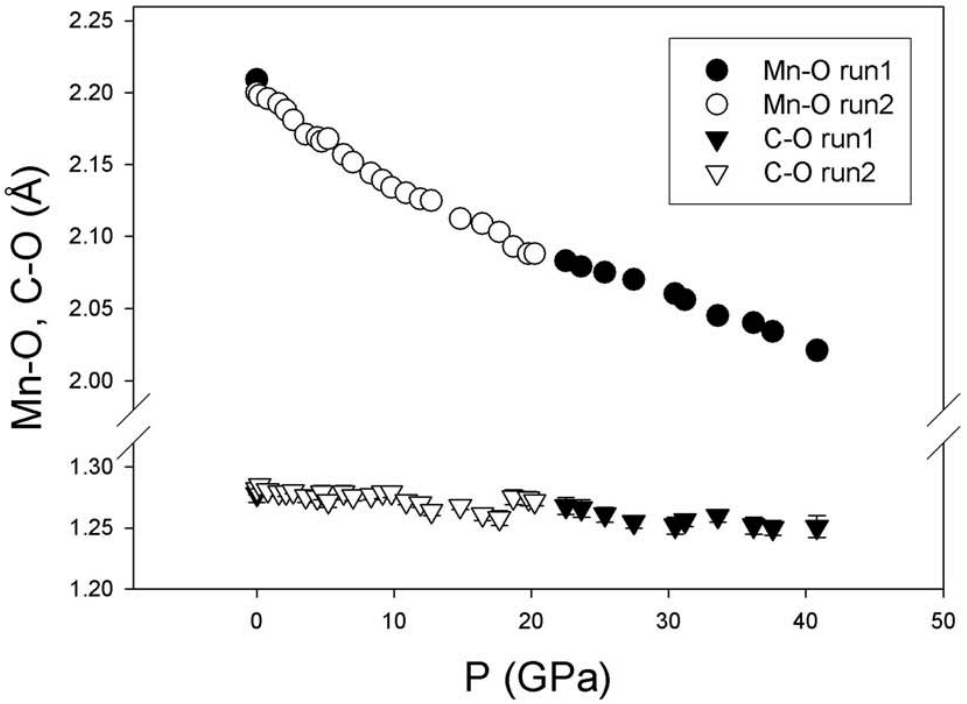
Mn-O run1
Mn-O run2
C-O run1
C-O run2
Mn-O, C-O (Å)
P (GPa)
2.25
2.20
2.15
2.10
2.05
2.00
1.30
1.25
1.20
0
10
20
30
40
50

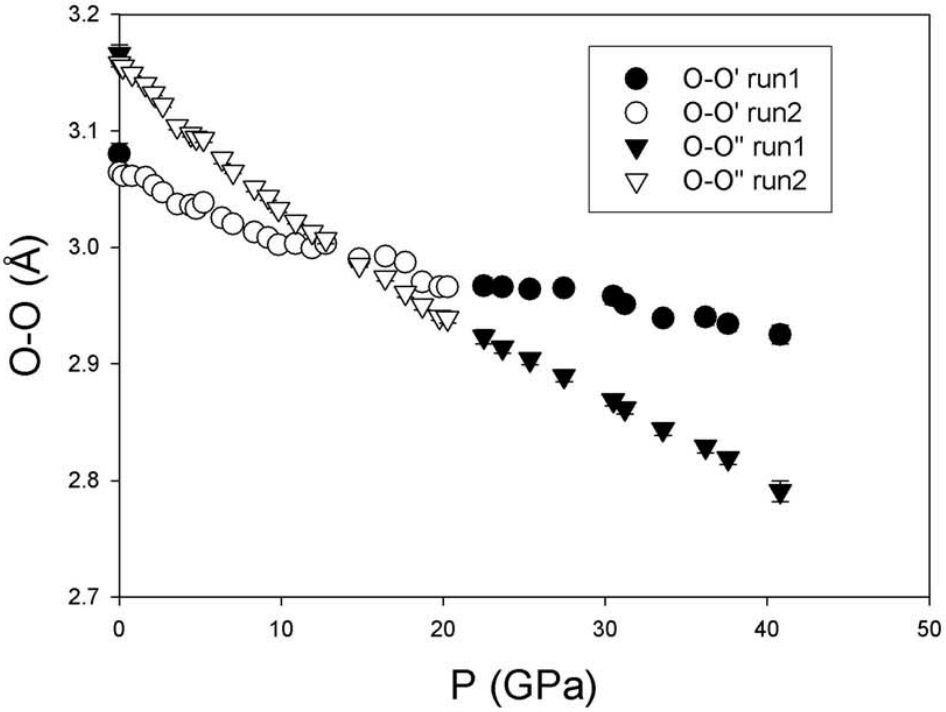
O-O' run1
O-O' run2
O-O'' run1
O-O'' run2
O-O (Å)
P (GPa)
3.2
3.1
3.0
2.9
2.8
2.7
0
10
20
30
40
50

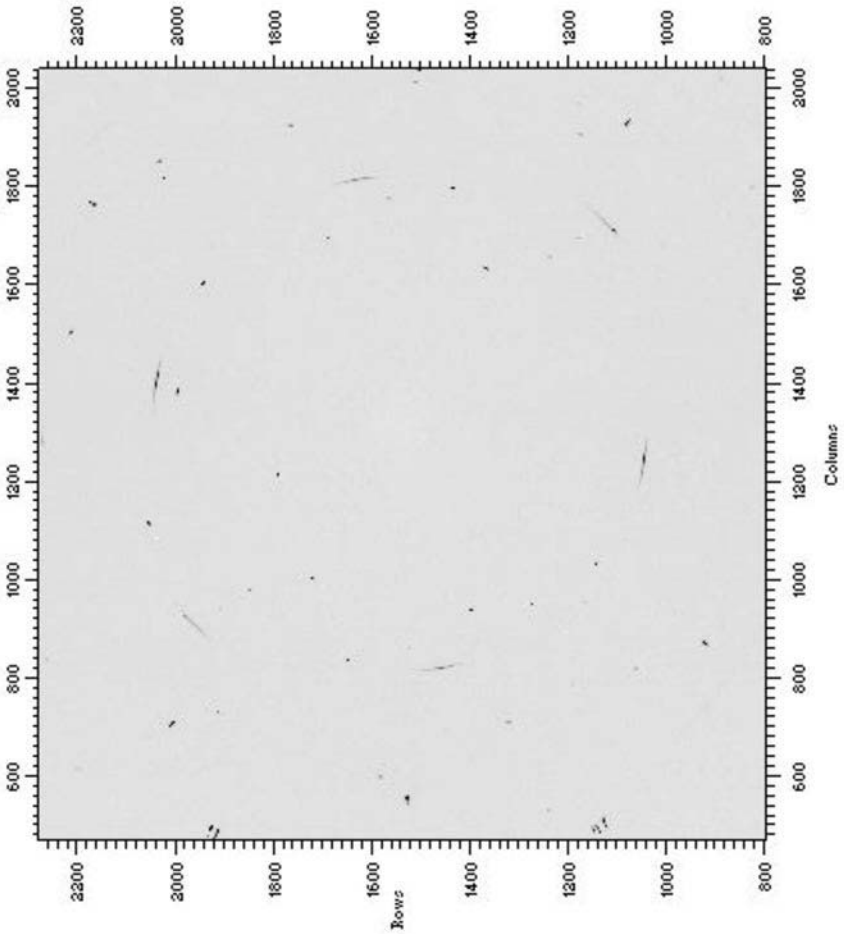
2200
2000
1800
1600
1400
1200
1000
800
600
Rows
Columns

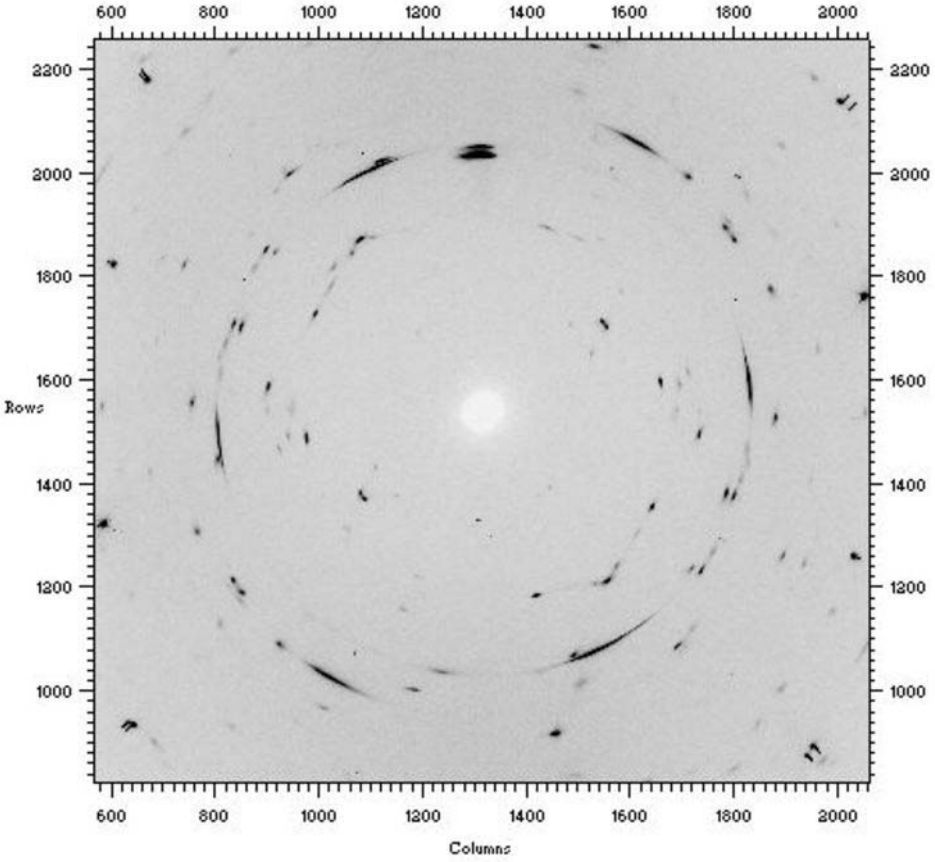
600
800
1000
1200
1400
1600
1800
2000
2200
Rows
Columns

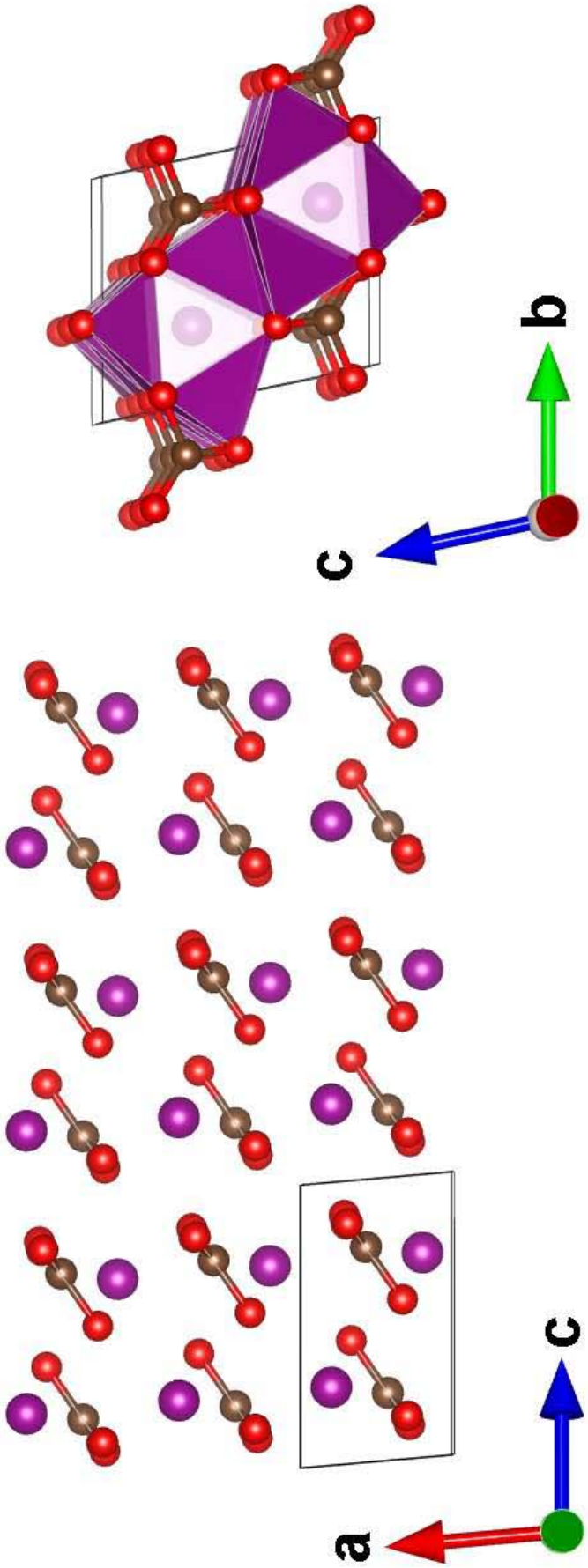
a
c
c
b

Table 1 – Crystallographic data of $MnCO_3$. *after 1 day. †only lattice parameter determination.

sample	P (Gpa)	a (Å)	c (Å)	V (Å^3)	V/Z (Å^3)	O_x	Mn-O (Å)	C-O (Å)	O1-O1' (Å)	O1-O1'' (Å)
run1-p0	0.0001	4.7903(10)	15.721(26)	312.4(4)	52.07(5)	0.2667(15)	2.209(5)	1.278(7)	3.080(9)	3.166(8)
run1-p1	22.50(5)	4.6581(9)	14.213(13)	267.1(2)	44.51(5)	0.2721(15)	2.083(4)	1.268(7)	2.967(7)	2.923(6)
run1-p2	23.65(5)	4.6554(9)	14.149(13)	265.6(2)	44.26(5)	0.2720(14)	2.079(4)	1.266(7)	2.966(6)	2.914(5)
run1-p3	25.34(5)	4.6473(9)	14.075(13)	263.3(2)	43.87(5)	0.2713(13)	2.075(3)	1.261(6)	2.964(6)	2.904(5)
run1-p4	27.45(5)	4.6416(9)	13.967(12)	260.6(2)	43.43(5)	0.2705(11)	2.070(3)	1.255(5)	2.965(5)	2.890(5)
run1-p5	30.48(5)	4.6302(14)	13.830(13)	256.8(2)	42.79(5)	0.2704(14)	2.060(4)	1.252(7)	2.958(7)	2.869(5)
run1-p6	31.19(5)	4.6278(14)	13.797(13)	255.9(2)	42.65(5)	0.2715(11)	2.056(3)	1.256(5)	2.951(5)	2.862(5)
run1-p7	33.56(5)	4.6193(14)	13.696(13)	253.1(2)	42.18(5)	0.2728(11)	2.045(3)	1.260(5)	2.939(5)	2.844(5)
run1-p8	36.20(5)	4.6100(14)	13.582(12)	245.0(2)	41.66(5)	0.2715(14)	2.040(4)	1.252(7)	2.940(7)	2.829(5)
run1-p9	37.58(5)	4.6024(14)	13.517(12)	248.0(2)	41.33(5)	0.2716(13)	2.034(4)	1.250(6)	2.934(6)	2.819(5)
run1-p10	40.80(5)	4.5927(14)	13.332(12)	243.5(1)	40.59(5)	0.2723(19)	2.021(5)	1.251(9)	2.925(8)	2.791(9)
run1-p11	44.46(5)	a=2.936(2)	α=100.82(6)	77.44(9)	38.72(5)		2.10(3)	1.27(4)		
		b=4.841(4)	β=94.93(6)							
		c=5.568(4)	γ=90.18(6)							
run1-p11*	46.79(5)	a=2.928(2)	α=101.71(6)	76.28(10)	38.14(5)		2.12(3)	1.26(5)		
		b=4.816(4)	β=94.99(6)							
		c=5.545(4)	γ=89.90(6)							
run1-p12	44.01(5)	a=2.934(2)	α=101.87(7)	76.88(11)	38.44(5)		2.14(6)	1.23(6)		
		b=4.839(4)	β=95.29(7)							
		c=5.557(4)	γ=89.73(7)							
run1-p13	41.55(5)	a=2.940(2)	α=101.99(6)	77.59(10)	38.80(5)		2.13(4)	1.24(5)		
		b=4.856(4)	β=95.58(6)							
		c=5.584(4)	γ=89.65(6)							
run1-p14	35.67(5)	a=2.9539(19)	α=100.78(5)	78.19(8)	39.10(5)		2.09(6)	1.24(8)		
		b=4.843(3)	β=95.09(5)							
		c=5.588(3)	γ=90.45(5)							
run1-p15†	33.17(5)	4.6332(9)	13.561(11)	252.1(2)	42.01(5)					
run1-p16†	29.86(5)	4.6330(9)	13.857(12)	257.6(2)	42.93(5)					
run1-p17†	24.34(5)	4.6524(9)	14.226(13)	266.7(2)	44.44(5)					
run1-p18†	18.59(5)	4.6824(10)	14.462(13)	274.6(2)	45.76(5)					
run1-p19†	8.03(5)	4.7301(10)	15.162(15)	293.8(3)	48.96(5)					
run2-p0	0.0001	4.7799(11)	15.694(6)	310.5(4)	51.75(5)	0.2684(9)	2.200(2)	1.282(5)	3.064(5)	3.158(3)
run2-p1	0.22(5)	4.7788(7)	15.685(4)	310.2(3)	51.70(5)	0.2689(7)	2.1980(18)	1.285(3)	3.061(5)	3.155(2)
run2-p2	0.79(5)	4.7753(3)	15.6360(16)	308.8(3)	51.46(5)	0.2683(7)	2.1959(18)	1.281(4)	3.061(5)	3.149(2)
run2-p3	1.62(5)	4.7714(4)	15.578(2)	307.1(3)	51.19(5)	0.2681(7)	2.1924(16)	1.279(3)	3.060(4)	3.140(2)
run2-p4	2.12(5)	4.7654(4)	15.531(2)	305.4(3)	50.91(5)	0.2684(6)	2.1876(15)	1.279(3)	3.053(3)	3.132(2)
run2-p5	2.66(5)	4.7581(4)	15.473(2)	303.4(3)	50.56(5)	0.2689(8)	2.181(2)	1.280(2)	3.047(4)	3.122(2)
run2-p6	3.57(5)	4.7426(3)	15.368(2)	299.3(3)	49.89(5)	0.2690(11)	2.171(3)	1.276(5)	3.037(5)	3.104(3)
run2-p7	4.39(5)	4.7409(3)	15.3191(15)	298.2(3)	49.70(5)	0.2690(8)	2.1685(19)	1.275(4)	3.036(4)	3.097(2)
run2-p8	4.74(5)	4.7415(4)	15.308(2)	298.0(4)	49.67(5)	0.2697(12)	2.166(3)	1.279(6)	3.033(6)	3.094(4)
run2-p9	5.20(5)	4.7388(5)	15.287(3)	297.3(4)	49.55(5)	0.2684(11)	2.168(2)	1.272(5)	3.038(4)	3.093(3)
run2-p10	6.33(5)	4.7332(3)	15.1926(19)	294.8(3)	49.13(5)	0.2701(13)	2.157(3)	1.279(6)	3.025(6)	3.076(4)
run2-p11	7.01(5)	4.7248(3)	15.1242(18)	292.4(3)	48.73(5)	0.2701(8)	2.1515(19)	1.276(4)	3.020(4)	3.065(2)
run2-p12	8.33(5)	4.7177(4)	15.043(2)	289.9(3)	48.32(5)	0.2707(9)	2.144(2)	1.277(4)	3.013(4)	3.051(3)
run2-p13	9.17(5)	4.7146(3)	14.9903(19)	288.6(4)	48.09(5)	0.2713(11)	2.139(3)	1.279(5)	3.008(4)	3.043(3)
run2-p14	9.82(5)	4.7087(3)	14.9313(17)	286.7(3)	47.78(5)	0.2716(9)	2.134(2)	1.279(4)	3.002(4)	3.033(3)
run2-p15	10.88(5)	4.7017(6)	14.855(4)	284.4(3)	47.40(5)	0.2706(6)	2.1303(16)	1.272(3)	3.003(3)	3.022(2)
run2-p16	11.90(5)	4.6955(3)	14.7918(17)	282.4(3)	47.07(5)	0.2705(5)	2.126(2)	1.270(3)	2.999(2)	3.013(2)
run2-p17	12.73(5)	4.6929(3)	14.7382(19)	281.1(3)	46.85(5)	0.2694(9)	2.125(2)	1.264(4)	3.003(4)	3.007(4)
run2-p18	14.82(5)	4.6826(3)	14.613(2)	277.5(3)	46.25(5)	0.2708(7)	2.1123(17)	1.268(3)	2.990(3)	2.985(2)
run2-p19	16.42(5)	4.6775(3)	14.528(2)	275.3(3)	45.88(5)	0.2696(11)	2.109(3)	1.261(5)	2.992(5)	2.974(3)
run2-p20	17.66(5)	4.6679(2)	14.4441(15)	272.6(3)	45.43(5)	0.2695(13)	2.103(3)	1.258(6)	2.987(6)	2.961(4)
run2-p21	18.69(5)	4.6686(4)	14.401(3)	271.8(4)	45.30(5)	0.2730(12)	2.093(3)	1.275(6)	2.970(6)	2.950(4)
run2-p22	19.78(5)	4.6641(12)	14.341(7)	270.2(3)	45.03(5)	0.2731(11)	2.088(3)	1.274(6)	2.966(5)	2.940(3)
run2-p23	20.24(5)	4.6624(18)	14.330(11)	269.8(3)	44.96(5)	0.2728(8)	2.088(3)	1.272(4)	2.966(4)	2.939(4)

Table 1 – Crystallographic data of $MnCO_3$. *after 1 day. †only lattice parameter determination.

sample	P (Gpa)	a (Å)	c (Å)	V (Å^3)	V/Z (Å^3)	O_x	Mn-O (Å)	C-O (Å)	O1-O1' (Å)	O1-O1'' (Å)
run1-p0	0.0001	4.7903(10)	15.721(26)	312.4(4)	52.07(5)	0.2667(15)	2.209(5)	1.278(7)	3.080(9)	3.166(8)
run1-p1	22.50(5)	4.6581(9)	14.213(13)	267.1(2)	44.51(5)	0.2721(15)	2.083(4)	1.268(7)	2.967(7)	2.923(6)
run1-p2	23.65(5)	4.6554(9)	14.149(13)	265.6(2)	44.26(5)	0.2720(14)	2.079(4)	1.266(7)	2.966(6)	2.914(5)
run1-p3	25.34(5)	4.6473(9)	14.075(13)	263.3(2)	43.87(5)	0.2713(13)	2.075(3)	1.261(6)	2.964(6)	2.904(5)
run1-p4	27.45(5)	4.6416(9)	13.967(12)	260.6(2)	43.43(5)	0.2705(11)	2.070(3)	1.255(5)	2.965(5)	2.890(5)
run1-p5	30.48(5)	4.6302(14)	13.830(13)	256.8(2)	42.79(5)	0.2704(14)	2.060(4)	1.252(7)	2.958(7)	2.869(5)
run1-p6	31.19(5)	4.6278(14)	13.797(13)	255.9(2)	42.65(5)	0.2715(11)	2.056(3)	1.256(5)	2.951(5)	2.862(5)
run1-p7	33.56(5)	4.6193(14)	13.696(13)	253.1(2)	42.18(5)	0.2728(11)	2.045(3)	1.260(5)	2.939(5)	2.844(5)
run1-p8	36.20(5)	4.6100(14)	13.582(12)	245.0(2)	41.66(5)	0.2715(14)	2.040(4)	1.252(7)	2.940(7)	2.829(5)
run1-p9	37.58(5)	4.6024(14)	13.517(12)	248.0(2)	41.33(5)	0.2716(13)	2.034(4)	1.250(6)	2.934(6)	2.819(5)
run1-p10	40.80(5)	4.5927(14)	13.332(12)	243.5(1)	40.59(5)	0.2723(19)	2.021(5)	1.251(9)	2.925(8)	2.791(9)
run1-p11	44.46(5)	a=2.936(2)	α=100.82(6)	77.44(9)	38.72(5)		2.10(3)	1.27(4)		
		b=4.841(4)	β=94.93(6)							
		c=5.568(4)	γ=90.18(6)							
run1-p11*	46.79(5)	a=2.928(2)	α=101.71(6)	76.28(10)	38.14(5)		2.12(3)	1.26(5)		
		b=4.816(4)	β=94.99(6)							
		c=5.545(4)	γ=89.90(6)							
run1-p12	44.01(5)	a=2.934(2)	α=101.87(7)	76.88(11)	38.44(5)		2.14(6)	1.23(6)		
		b=4.839(4)	β=95.29(7)							
		c=5.557(4)	γ=89.73(7)							
run1-p13	41.55(5)	a=2.940(2)	α=101.99(6)	77.59(10)	38.80(5)		2.13(4)	1.24(5)		
		b=4.856(4)	β=95.58(6)							
		c=5.584(4)	γ=89.65(6)							
run1-p14	35.67(5)	a=2.9539(19)	α=100.78(5)	78.19(8)	39.10(5)		2.09(6)	1.24(8)		
		b=4.843(3)	β=95.09(5)							
		c=5.588(3)	γ=90.45(5)							
run1-p15†	33.17(5)	4.6332(9)	13.561(11)	252.1(2)	42.01(5)					
run1-p16†	29.86(5)	4.6330(9)	13.857(12)	257.6(2)	42.93(5)					
run1-p17†	24.34(5)	4.6524(9)	14.226(13)	266.7(2)	44.44(5)					
run1-p18†	18.59(5)	4.6824(10)	14.462(13)	274.6(2)	45.76(5)					
run1-p19†	8.03(5)	4.7301(10)	15.162(15)	293.8(3)	48.96(5)					
run2-p0	0.0001	4.7799(11)	15.694(6)	310.5(4)	51.75(5)	0.2684(9)	2.200(2)	1.282(5)	3.064(5)	3.158(3)
run2-p1	0.22(5)	4.7788(7)	15.685(4)	310.2(3)	51.70(5)	0.2689(7)	2.1980(18)	1.285(3)	3.061(5)	3.155(2)
run2-p2	0.79(5)	4.7753(3)	15.6360(16)	308.8(3)	51.46(5)	0.2683(7)	2.1959(18)	1.281(4)	3.061(5)	3.149(2)
run2-p3	1.62(5)	4.7714(4)	15.578(2)	307.1(3)	51.19(5)	0.2681(7)	2.1924(16)	1.279(3)	3.060(4)	3.140(2)
run2-p4	2.12(5)	4.7654(4)	15.531(2)	305.4(3)	50.91(5)	0.2684(6)	2.1876(15)	1.279(3)	3.053(3)	3.132(2)
run2-p5	2.66(5)	4.7581(4)	15.473(2)	303.4(3)	50.56(5)	0.2689(8)	2.181(2)	1.280(2)	3.047(4)	3.122(2)
run2-p6	3.57(5)	4.7426(3)	15.368(2)	299.3(3)	49.89(5)	0.2690(11)	2.171(3)	1.276(5)	3.037(5)	3.104(3)
run2-p7	4.39(5)	4.7409(3)	15.3191(15)	298.2(3)	49.70(5)	0.2690(8)	2.1685(19)	1.275(4)	3.036(4)	3.097(2)
run2-p8	4.74(5)	4.7415(4)	15.308(2)	298.0(4)	49.67(5)	0.2697(12)	2.166(3)	1.279(6)	3.033(6)	3.094(4)
run2-p9	5.20(5)	4.7388(5)	15.287(3)	297.3(4)	49.55(5)	0.2684(11)	2.168(2)	1.272(5)	3.038(4)	3.093(3)
run2-p10	6.33(5)	4.7332(3)	15.1926(19)	294.8(3)	49.13(5)	0.2701(13)	2.157(3)	1.279(6)	3.025(6)	3.076(4)
run2-p11	7.01(5)	4.7248(3)	15.1242(18)	292.4(3)	48.73(5)	0.2701(8)	2.1515(19)	1.276(4)	3.020(4)	3.065(2)
run2-p12	8.33(5)	4.7177(4)	15.043(2)	289.9(3)	48.32(5)	0.2707(9)	2.144(2)	1.277(4)	3.013(4)	3.051(3)
run2-p13	9.17(5)	4.7146(3)	14.9903(19)	288.6(4)	48.09(5)	0.2713(11)	2.139(3)	1.279(5)	3.008(4)	3.043(3)
run2-p14	9.82(5)	4.7087(3)	14.9313(17)	286.7(3)	47.78(5)	0.2716(9)	2.134(2)	1.279(4)	3.002(4)	3.033(3)
run2-p15	10.88(5)	4.7017(6)	14.855(4)	284.4(3)	47.40(5)	0.2706(6)	2.1303(16)	1.272(3)	3.003(3)	3.022(2)
run2-p16	11.90(5)	4.6955(3)	14.7918(17)	282.4(3)	47.07(5)	0.2705(5)	2.126(2)	1.270(3)	2.999(2)	3.013(2)
run2-p17	12.73(5)	4.6929(3)	14.7382(19)	281.1(3)	46.85(5)	0.2694(9)	2.125(2)	1.264(4)	3.003(4)	3.007(4)
run2-p18	14.82(5)	4.6826(3)	14.613(2)	277.5(3)	46.25(5)	0.2708(7)	2.1123(17)	1.268(3)	2.990(3)	2.985(2)
run2-p19	16.42(5)	4.6775(3)	14.528(2)	275.3(3)	45.88(5)	0.2696(11)	2.109(3)	1.261(5)	2.992(5)	2.974(3)
run2-p20	17.66(5)	4.6679(2)	14.4441(15)	272.6(3)	45.43(5)	0.2695(13)	2.103(3)	1.258(6)	2.987(6)	2.961(4)
run2-p21	18.69(5)	4.6686(4)	14.401(3)	271.8(4)	45.30(5)	0.2730(12)	2.093(3)	1.275(6)	2.970(6)	2.950(4)
run2-p22	19.78(5)	4.6641(12)	14.341(7)	270.2(3)	45.03(5)	0.2731(11)	2.088(3)	1.274(6)	2.966(5)	2.940(3)
run2-p23	20.24(5)	4.6624(18)	14.330(11)	269.8(3)	44.96(5)	0.2728(8)	2.088(3)	1.272(4)	2.966(4)	2.939(4)

Table 2 – Crystallographic data and selected interatomic distances for MnCO3-II at 46.8 GPa

Chemical formula	Mn C O_3
Space group	*P* -1 (no. 2)
Unit cell dimensions	*a* = 2.928(2) Å
	b = 4.816(4) Å
	c = 5.545(4) Å
	α = 101.71(7) °
	β = 94.99(7) °
	γ = 89.90(7) °
Cell volume	76.26(10) $Å^3$
Z	2
R(Brgg) %	6.48

Atom	**x**	**y**	**z**	**U ($Å^2$)**
Mn1	0.199(2)	0.307(1)	0.724(1)	0.013(4)
O1	0.697(13)	0.045(8)	0.849(5)	0.021(3)
O2	0.716(9)	0.595(6)	0.880(3)	0.002(2)
O3	-0.335(11)	0.236(6)	0.436(4)	0.015(3)
C1	0.575(15)	0.788(9)	0.760(5)	0.010(3)

Mn1	O2	2.07(4)
	O1	2.09(3)
	O2	2.09(3)
	O3	2.11(3)
	O2	2.14(2)
	O3	2.17(2)
	O1	2.18(3)
	O3	2.58(4)
	O3	2.62(3)
C1	O3	1.22(4)
	O1	1.27(6)
	O2	1.30(5)

Supplementary materials

Table S1 – Statistic agreement factors for all the structural refinements performed with the Jana2006 software

	R(obs)	wR(obs)	R(all)	wR(all)
run1-p0	6.57	7.49	7.07	7.51
run1-p1	6.02	6.51	7.48	6.59
run1-p2	6.33	7.09	6.99	7.16
run1-p3	5.67	6.65	6.07	6.66
run1-p4	4.68	5.43	5.24	5.45
run1-p5	4.87	6.16	5.62	6.2
run1-p6	4.44	5.08	4.93	5.09
run1-p7	4.73	5.44	5.06	5.46
run1-p8	5.29	6.22	5.41	6.22
run1-p9	4	5.54	4.33	5.56
run1-p10	5.64	5.65	7.74	5.93
run1-p11	6.48	6.84	8.46	7.05
run1-p11*	7.65	7.99	8.53	8.03
run1-p12	7.22	8.55	8.21	8.77
run1-p13	7.8	9.11	8.64	9.24
run1-p14	8.84	9.96	9.52	9.99
run2-p0	4.4	5.15	5.04	5.17
run2-p1	2.56	3.83	2.86	3.84
run2-p2	3.12	3.84	3.33	3.85
run2-p3	3.14	3.37	3.68	3.44
run2-p4	2.86	3.16	3.22	3.19
run2-p5	3.62	4.07	3.91	4.08
run2-p6	5.11	4.93	5.37	4.94
run2-p7	3.69	4.07	4.57	4.09
run2-p8	5.5	5.75	6.78	6.13
run2-p9	4.32	4.8	4.71	4.81
run2-p10	5.41	5.97	5.78	6
run2-p11	2.77	3.43	3.04	3.44
run2-p12	3.46	4.08	3.66	4.09
run2-p13	4.26	4.85	4.67	4.87
run2-p14	3.51	4.17	3.76	4.18
run2-p15	2.79	3.55	2.95	3.55
run2-p16	2.09	2.85	2.24	2.86
run2-p17	3.53	4.34	3.65	4.34
run2-p18	2.74	3.5	3.36	3.7
run2-p19	4.58	5.59	4.73	5.59
run2-p20	5.53	5.87	6.47	5.94
run2-p21	5.15	5.04	7.07	5.33
run2-p22	4.11	4.78	4.6	4.8
run2-p23	3.51	4.13	3.92	4.15

Table S2 – Crystallographic data of MnCO3-II

P step	P (Gpa)	atom	x	y	z	Uiso (Å ^{2})
run1-p11	44.46(5)	Mn1	0.197(2)	0.3078(13)	0.7281(9)	0.017(3)
		O1	0.734(8)	0.064(5)	0.825(3)	0.009(2)
		O2	0.721(8)	0.614(6)	0.875(4)	0.014(3)
		O3	-0.295(9)	0.253(5)	0.420(4)	0.015(3)
		C1	0.567(10)	0.800(7)	0.770(5)	0.007(3)
run1-p11*	46.79(5)	Mn1	0.199(2)	0.3067(14)	0.7244(10)	0.012(5)
		O1	0.697(13)	0.045(8)	0.849(5)	0.021(4)
		O2	0.716(9)	0.595(6)	0.880(4)	0.002(2)
		O3	-0.335(11)	0.236(7)	0.436(4)	0.015(4)
		C1	0.575(15)	0.788(10)	0.760(6)	0.010(4)
run1-p12	44.01(5)	Mn1	0.193(4)	0.303(2)	0.7264(12)	0.026(5)
		O1	0.693(17)	0.042(10)	0.855(6)	0.022(4)
		O2	0.719(9)	0.608(5)	0.867(4)	0.004(3)
		O3	-0.350(12)	0.233(6)	0.436(5)	0.024(4)
		C1	0.589(18)	0.804(10)	0.766(8)	0.032(6)
run1-p13	41.55(5)	Mn1	0.195(4)	0.306(2)	0.7257(13)	0.037(6)
		O1	0.70(2)	0.048(12)	0.846(8)	0.030(6)
		O2	0.729(9)	0.617(5)	0.863(4)	0.006(3)
		O3	-0.337(11)	0.242(6)	0.431(4)	0.018(3)
		C1	0.635(15)	0.846(9)	0.735(7)	0.022(5)
run1-p14	35.67(5)	Mn1	0.199(4)	0.307(2)	0.7262(14)	0.036(6)
		O1	0.68(2)	0.038(12)	0.845(8)	0.025(5)
		O2	0.704(11)	0.599(7)	0.866(5)	0.004(3)
		O3	-0.313(18)	0.266(10)	0.434(6)	0.013(4)
		C1	0.59(3)	0.812(18)	0.780(12)	0.030(8)

Table S3 – Axial compressibility of MnCO3, calculated using the cube of a and c lattice parameters

K_0a 227(7) GPa	a_0^3 108.92(13) $Å^3$
K_0c 39(1)	c_{03} 3948(15) $Å^3$

Figure S1 – f-F plot for MnCO3 in the pressure range 0-40 GPa. The plot suggest that a 2nd or a 3rd (with K'<4 and close to 4) order Birch-Murnagham Equation of State is appropriate for fitting the volume data at various pressures.